Allosteric cooperativity in protein kinase A

Larry R. Masterson*, Alessandro Mascioni*, Nathaniel J. Traaseth*, Susan S. Taylor[†‡], and Gianluigi Veglia*[‡§]

Departments of *Chemistry and [§]Biochemistry, Molecular Biology, and Biophysics, University of Minnesota, Minneapolis, MN 55455; and [†]Department of Chemistry and Biochemistry, University of California at San Diego, La Jolla, CA 92093

Contributed by Susan S. Taylor, September 28, 2007 (sent for review March 12, 2007)

Allosteric signaling in proteins requires long-range communication mediated by highly conserved residues, often triggered by ligand binding. In this article, we map the allosteric network in the catalytic subunit of protein kinase A using NMR spectroscopy. We show that positive allosteric cooperativity is generated by nucleotide and substrate binding during the transitions through the major conformational states: apo, intermediate, and closed. The allosteric network is disrupted by a single site mutation (Y204A), which also decouples the cooperativity of ligand binding. Because protein kinase A is the prototype for the entire kinome, these findings may serve as a paradigm for describing long-range coupling in other protein kinases.

allostery | NMR | signaling | enzymes | chemical shift mapping

The protein kinase superfamily is one of the largest gene families in eukaryotes, representing 2–4% of most genomes (1, 2). The human genome, for example, has >500 predicted protein kinases. Protein kinases relay an extracellular signal into a biological response by phosphoryl transfer on specific substrates resulting in regulation of cell division, memory, differentiation, cell growth, and most other cell processes with exquisite precision. Since the first structure of the catalytic subunit of protein kinase A (PKA-C) was determined in 1991 (3, 4), there has been significant progress in filling the structural space of this family. Over 60 unique kinase structures are now available in the Protein Data Bank (PDB; www.rcsb.org). All of these structures share a highly conserved kidney-shaped core that in PKA-C comprises residues 40–300. The core consists of a small N-terminal lobe formed by β-strands that binds and positions ATP during catalysis and a large lobe that provides a docking surface for the substrate. The N terminus ends with a single helix of $\approx$40 residues (A helix). The 50 residues comprising the C terminus wrap around the two lobes, docking into a hydrophobic pocket located in the small lobe (3, 4).

Despite sharing a highly conserved core, protein kinases are remarkably diverse in terms of their regulation, activation, and substrate recognition. Crystal structures suggest that kinases are highly dynamic, with allosteric networks that radiate throughout the molecule. Unfortunately, these structures are static and often only include the kinase core. Although there have been extensive studies of kinases in solution, including hydrogen/deuterium exchange coupled with mass spectrometry (H/D-MS), fluorescence anisotropy (5–7), and small-angle x-ray scattering (8, 9), these results lack atomic-level resolution and offer an incomplete picture of protein dynamics and recognition mechanisms, presenting a substantial limitation in understanding the enzymatic cycle of kinases, and leaving many questions unanswered. How do these enzymes discriminate cognate and noncognate substrates? What is the role of the nucleotide in substrate recognition? Does allostery play a fundamental role in these recognition processes?

Here, we analyze the transitions between the major states of the intact PKA-C (apo, intermediate, and closed) using NMR spectroscopy under functional conditions. This detailed residue-by-residue analysis revealed the existence of positive allosteric cooperativity, which is triggered by ligand binding. NMR chemical-shift mapping showed that a single mutation (Y204A) in the peptide-positioning loop is able to disturb the allosteric network and decouple the cooperativity.

Results

NMR Spectroscopy of the Major Conformational States. The chemical-shift changes in PKA-C upon ligand binding were monitored by using 2D $^{1}H/^{15}N$ TROSY–heteronuclear single quantum coherence (HSQC) (10) spectra. To mimic ATP, the nonhydrolyzable nucleotide 5′-adenylyl-β,γ-imidodiphosphate (AMP-PNP) was used. The AMP-PNP-saturated enzyme was then titrated with Kemptide to mimic the Michaelis complex. Fig. 1 shows the spectra of the four distinct conformational states of the C-subunit: apo, intermediate-N (enzyme saturated with nucleotide), intermediate-S (enzyme saturated with substrate), and closed. A total of 253 of 337 expected amide peaks were suitable for chemical-shift perturbation ($\Delta\delta$) and lineshape analyses. These peaks are well distributed across the protein, giving an overall view of the enzyme's behavior during ligand binding. Although the majority of the peaks displayed fast exchange upon ligand binding, several of the resonances were exchange-broadened under saturating ligand conditions, supporting the existence of multiple conformational states and a complex energy landscape for the enzyme (11, 12).

In the following synopsis, we describe the changes in the HSQC fingerprint data of the wild-type and Y204A mutant of PKA-C upon addition of nucleotide and substrate.

AMP-PNP Binding. Fig. 2 summarizes the chemical-shift perturbations occurring at each amide site upon AMP-PNP binding. As expected for AMP-PNP binding, a cluster of residues within the small lobe of the enzyme is highly sensitive to the addition of nucleotide. The most pronounced changes ($\Delta\delta > 0.05$ ppm) are observed in residues of the β3-strand and the highly conserved glycine-rich loop (β1- and β2-strands), which actively participate in positioning the nucleotide. Crystal structures have shown that the β3-strand flanks the nucleotide-binding site and contains K72, which coordinates the α- and β-phosphates of ATP (13, 14). Gradual decreases of $\Delta\delta$ toward the C- and N-terminal regions from the glycine-rich loop suggest that nucleotide binding affects distal sites within the small lobe of the enzyme. This is evident by the large $\Delta\delta$ values for residues that in the crystal structure are >35 Å away from helices A and B (Fig. 3).

A second region is centered at A188 and at the surface of the large lobe where substrate docking would take place (Figs. 2 and 3). This large perturbation is important, because crystal structures reveal that the A188 amide group points toward the substrate recognition sequence (15). This region contains highly conserved loops, including the DFG loop, which has been proposed to be a switch between active and inactive kinase

Author contributions: G.V. designed research; L.R.M., A.M., and N.J.T. performed research; S.S.T. analyzed data; and G.V. wrote the paper.

The authors declare no conflict of interest.

[‡]To whom correspondence may be addressed. E-mail: staylor@ucsd.edu or veglia@chem.umn.edu.

This article contains supporting information online at www.pnas.org/cgi/content/full/0709214104/DC1.

© 2008 by The National Academy of Sciences of the USA

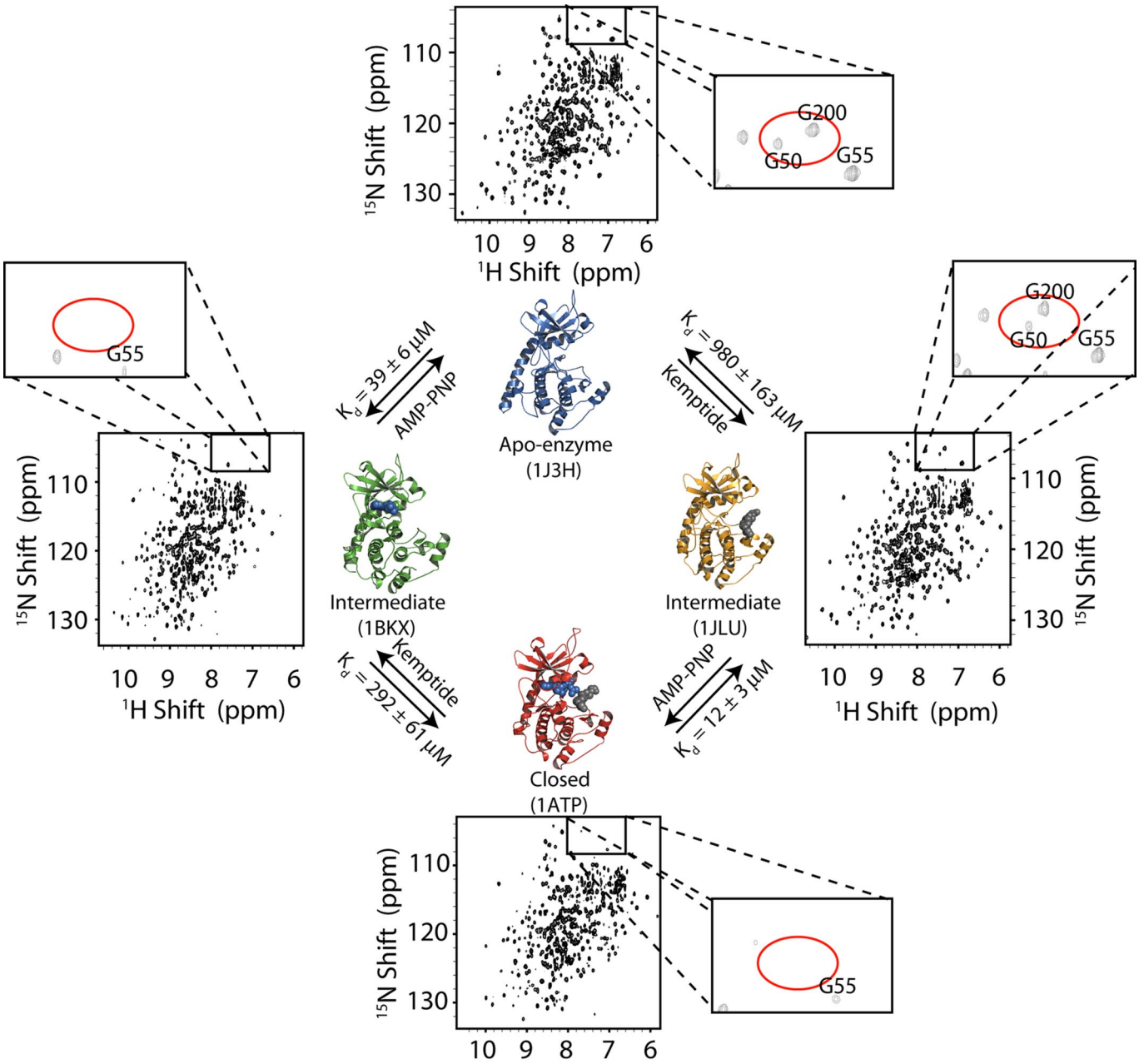

Fig. 1. ^{1}H/^{15}N TROSY-HSQC spectra obtained for the conformational states of PKA-C: apo (*Upper*), intermediate-N (*Left*), intermediate-S (*Right*), and closed (*Lower*). Expanded boxes highlight residues of the glycine-rich and peptide-positioning loops. Titrations with AMP-PNP first were performed with 0.63 mM C-subunit, and titrations using Kemptide first were performed with 0.44 mM C-subunit.

conformations (16). The resonances belonging to the DFG loop (F185, G186, and F187) were broadened beyond detection (see *, Fig. 2), indicating conformational interconversion between multiple states, which were silent to the x-ray analysis. Significant changes are observed for residues T201 and G200, which became exchange-broadened; these residues are conserved throughout the Ser/Thr kinase family (17). The large perturbations at the peptide positioning loop, with concomitant changes in the DFG- and glycine-rich loops, reveal that the nucleotide affects both the small and large lobes, perhaps priming the enzyme for substrate binding. This is supported by x-ray studies carried out by Johnson *et al.* (18) that show ligand-induced conformational changes at these domains. The F helix located near the peptide-positioning loop also has large $\Delta\delta$ values that gradually decrease toward the C terminus where a third region is sensitive to binding. The large $\Delta\delta$ values for residues at the C terminus reflect the structural features of the enzyme highlighted in Fig. 3; the C terminus wraps around the small lobe of the enzyme and positions F325–E337 near the glycine-rich loop (19). Marked changes along the primary sequence in the large lobe (including the F–J helices) suggest that nucleotide binding radiates its effects to distal sites of both lobes.

Kemptide Binding. After saturation with the nucleotide (i.e., formation of intermediate-N), Kemptide was titrated into the sample to mimic the closed state (Michaelis complex). Whereas AMP-PNP caused large $\Delta\delta$ throughout the enzyme (≈30% of the assigned residues have $\Delta\delta > 0.05$), the perturbations observed upon binding Kemptide are significantly lower ($\langle\Delta\delta\rangle$ =

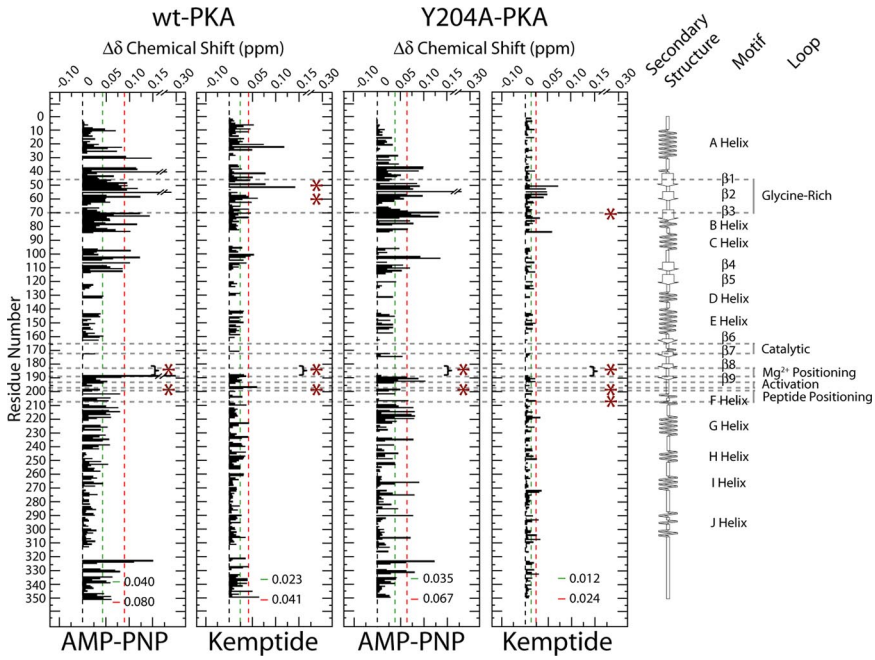

Fig. 2. Residue specific perturbations observed during ligand binding. Histograms show the combined $^{1}H/^{15}N$ chemical shift perturbations ($\Delta\delta = \sqrt{\Delta\delta_H^2 + (0.154\Delta\delta N)^2}$) vs. residue. The cutoffs for $\langle\Delta\delta\rangle$ and $\langle\Delta\delta\rangle$ plus 1 SD are given as green and red dashed lines, respectively. Asterisks indicate exchange broadened residues.

0.023), with <8% of the residues perturbed >0.05 ppm. Residue-specific differences are evident in Fig. 2, but the overall pattern of Δδ for the Kemptide titration is similar to that of the nucleotide. The most prominent perturbations are localized in three regions: in the glycine-rich loop, between the catalytic and the peptide-positioning loops, and the C-terminal portion of the enzyme. The largest perturbation occurs at S53, which in the crystal structures bridges the nucleotide and substrate. The backbone amide interacts with the γ-phosphate of ATP, and its side chain hydroxyl group forms a hydrogen bond with the backbone carbonyl of the P-site residue of the substrate (15). A gradual decrease of Δδ was observed from the glycine-rich loop toward the N and C termini. Significant Δδ at distal sites of the small lobe again suggest sensitivity to binding, but here they are induced by changes at the surface of the large lobe.

Interestingly, the exchange broadening caused by nucleotide binding for residues in the DFG- and peptide-positioning loops persists under saturation with Kemptide. Additionally, G50 and G52 became exchange-broadened, supporting the existence of interconverting conformations. As with AMP-PNP, the extent of Δδ decreases from the F to the J helix. Small yet significant Δδ values may be indicative of a redistribution of the conformational energy upon substrate binding, an effect not anticipated from x-ray structures. Of course, Kemptide is a small substrate and the effects described could be further widespread or increased with larger substrates.

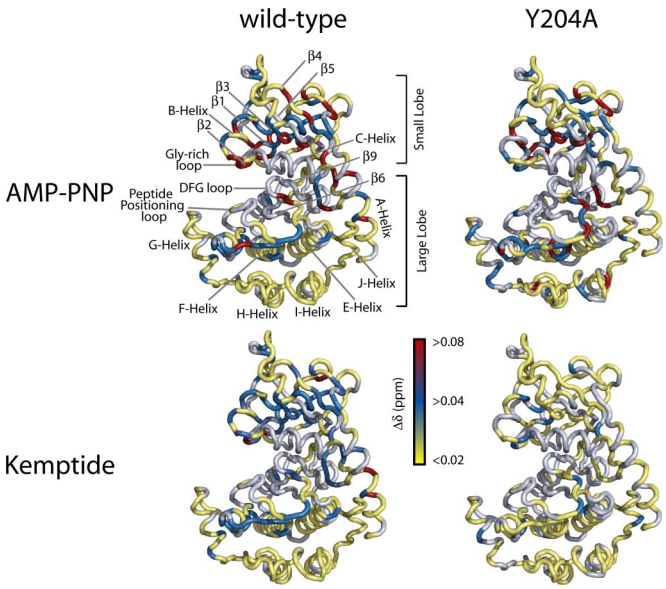

Fig. 3. Chemical-shift perturbation mapping. Perturbations were mapped for the nucleotide-bound (intermediate-N) and closed forms of wild-type (*Left*) and Y204A (*Right*) enzymes.

Reverse Order of Ligand Binding. The titrations were repeated by inverting the order of ligand additions, adding Kemptide first (i.e., intermediate-S) and then saturating the enzyme with AMP-PNP to form the Michaelis complex [the histograms with residue vs. Δδ number are provided in supporting information (SI) Fig. 5]. Unlike AMP-PNP addition to the apo-enzyme, saturation with Kemptide caused relatively modest changes to the enzyme fingerprint. Only the phosphorylated S10 located in the A helix shows a drastic chemical-shift change. However, smaller changes are detected throughout the entire enzyme's backbone, which indicates that Kemptide binding radiates its effects to both lobes. Subsequent addition of AMP-PNP to the Kemptide-bound enzyme caused changes in three regions that are similar to the direct titration: around the glycine-rich loop, between the catalytic and peptide-positioning loops, and the unstructured C-terminal portion of the enzyme (SI Fig. 5). Irrespective of the order of ligands used in the titrations, the 2D $^{1}H/^{15}N$ TROSY-HSQC spectra of the closed form of the enzyme are superimposable, which illustrates the thermodynamic equivalence for binding pathways.

Table 1. Binding constants (K_d, μM) measured from the NMR titrations of C-subunit PKA

Enzyme	AMP-PNP first		Kemptide first	
	$K_d^{AMP\text{-}PNP}$	$K_d^{Kemptide}$	$K_d^{Kemptide}$	$K_d^{AMP\text{-}PNP}$
wt-PKA	39 ± 6	292 ± 61	980 ± 163	12 ± 3
Y204A-PKA	78 ± 20	834 ± 92	700 ± 105	68 ± 4

Cooperativity of Ligand Binding. Resonances undergoing fast exchange were selected for the calculation of the dissociation constants (K_d). Table 1 summarizes the calculated K_d values, and representative fits are provided in SI Fig. 6. We measured a K_d of 39 ± 6 μM for AMP-PNP and an apparent K_d value of 292 ± 61 μM for Kemptide, which compares well with values reported for ATP (K_d = 25 ± 1 μM) and Ala-Kemptide (LRRAALG) (K_d = 230 ± 70 μM) attained by transient-state kinetic studies (20). The relative affinity of substrate and nucleotide was also examined from the reverse-order titration by using Kemptide first. In this case, the K_d for Kemptide was 980 ± 163 μM, and the apparent K_d for AMP-PNP was 12 ± 3 μM. Thus, binding of the first ligand appears to enhance the affinity of the second ligand, which corresponds to positive cooperativity.

Disruption of the Allosteric Network and Decoupling Positive Cooperativity. Is it possible to remove positive cooperativity by disrupting the allosteric network? To answer this question, we repeated the NMR titrations with the Y204A-PKA-C mutant. This mutation is located in the peptide-positioning loop and yet the enzyme binds ATP and a peptide inhibitor similar to the wild-type enzyme (21). However, solvent accessibility and thermostability studies have pointed to a disruption of the allosteric network, which likely causes the 30-fold decrease in the enzyme's turnover rate (22, 23). The direct titration using the nucleotide first resulted in a K_d value of 78 ± 20 μM and an apparent K_d value of 834 ± 92 μM for Kemptide. The reverse titration (Kemptide first) resulted in a K_d value of 700 ± 105 μM for Kemptide and an apparent K_d value of 68 ± 4 μM for AMP-PNP. The K_d values (Table 1) for the mutant show no cooperative binding effect, indicating that the two binding events have become decoupled.

Fig. 2 shows the $\Delta\delta$ upon the direct titration of AMP-PNP, whereas SI Fig. 5 shows the corresponding reverse titration. The overall trend of $\Delta\delta$ for AMP-PNP is similar to the wild type, with three regions primarily affected: the glycine-rich loop, the peptide-positioning loop, and the C terminus. However, these perturbations are attenuated and altered with respect to the wild-type enzyme. In particular, smaller changes were observed at the distal sites near the N-and C-terminal regions of the small lobe, residues 100–110, and the residues surrounding the peptide positioning loop of the large lobe. Fig. 3 illustrates two different allosteric networks of interactions between the wild-type and mutant enzymes. Although the chemical shift perturbations are more localized around the binding site of the wild-type enzyme, the allosteric effects induced by the nucleotide binding in Y204A are dispersed throughout the large lobe (see $\Delta\delta$ for helices G–J). The disruption of the allosteric network in Y204A is more apparent upon binding Kemptide, where modest chemical-shift changes throughout the protein backbone are observed. The only region showing significant perturbation is the glycine-rich loop, which is drastically attenuated compared with the wild-type enzyme. Moreover, the effects that radiated to distal sites in the small and large lobe are no longer present for Kemptide (Fig. 3).

Lineshape Analysis for Wild-Type PKA-C. Among all of the resolved amide resonances we isolated those experiencing an intermediate two-site exchange during AMP-PNP titrations and carried out a quantitative lineshape analysis to evaluate the binding kinetics. Because K_d values were independently measured from residues affected by fast exchange, we calculated both the on- and off-rates ($K_d = k_{off}/k_{on}$) by analyzing the NMR line-broadening dependence from k_{on}[ligand] and k_{off} (24). The lineshape analyses of five different peaks (F110, F108, F100, R190, and R93) resulted in on-rates for AMP-PNP ranging between 0.7 and 2.8 × 10^6 $M^{-1}\cdot s^{-1}$. Examples of lineshape fitting and a table reporting the k_{on} values for five residues are reported in SI Fig. 7 and SI Table 2). These on-rates are very similar to those reported for PKA-C using transient kinetic measurements (20). As for other enzymes (24, 25), k_{on} is ≈2 orders of magnitude lower than the bimolecular diffusion-controlled rates (≈10^8-10^9 $M^{-1}\cdot s^{-1}$). The low on-rates support the hypothesis of a rather complex binding mechanism for the nucleotide, which requires conformational changes in the small lobe (18). These changes within segments of the small lobe are thought to be responsible for binding, aligning, and positioning the nucleotide for the formation of a catalytically competent complex. In addition to this, changes in both lobes occur to properly position the substrate and shield the active site from bulk water (26).

Discussion

NMR spectroscopy is becoming the method of choice to analyze allostery (27–35), cooperativity (27, 32, 36–38), energy landscapes (11, 32, 36–38), and coordination of reactions for small and large enzymes (11, 38, 40). The first vivid picture of the complex changes occurring during the transitions from apo to intermediate and from intermediate to closed conformations in the backbone of PKA-C emerges from our NMR titrations. Specifically, the NMR characterization of allostery resulted in the identification of positive cooperativity for ligand binding. A key result in our data is the presence of exchange broadening for highly conserved residues in the kinase family (i.e., G50, G52, F185, G186, and G200) under saturating conditions of nucleotide or nucleotide plus substrate (see Figs. 1 and 2 and SI Fig. 6). This suggests that PKA-C interconverts between multiple dynamic or conformational states. Thus, it is possible that in solution, the conformational states identified by x-ray crystallography are in equilibrium. In the absence of ligands, the protein favors the conformation observed in the crystal structure of the apo state, with small populations of the other states. The addition of ligand alters this equilibrium to favor the intermediate and closed conformations. In this manner, the first ligand can drive the system close to the final state, facilitating binding of the second ligand.

To test the existence of the allosteric network, we mutated Y204 to A. Y204 is located in the P + 1 loop and is part of the tetrad of residues that keeps the F helix, D helix, and P-2-binding site together through electrostatic interactions (21, 23). This single mutation caused disruptions in the allosteric network and removed binding cooperativity. The comparison of our NMR titrations between the wild-type and Y204A mutant enzymes shows that this allostery is mediated by both local (contiguous) and long-range (non-contiguous or disperse) (41) changes. During the binding of nucleotide, we observed a cluster of hydrophobic residues (L59, A70, M120, and L106) that were particularly sensitive ($\Delta\delta$ ≈0.1 ppm) in the wild-type enzyme. These residues make contact with the evolutionarily conserved "spine" (L106, L95, F185, and Y164) recently identified by Kornev *et al.* (42), to form a hydrophobic lining about the adenine ring (Fig. 4). Sensing and positioning of the nucleotide at this region could act as a trigger for signaling, which is propagated across a network of residues away from the active site. Perturbations >0.05 ppm are traceable across conserved residues within van der Waals radii from the hydrophobic lining (Fig. 4). Several contiguous pathways of intramolecular cross-talk can also be traced from the hydrophobic lining to residues, which can

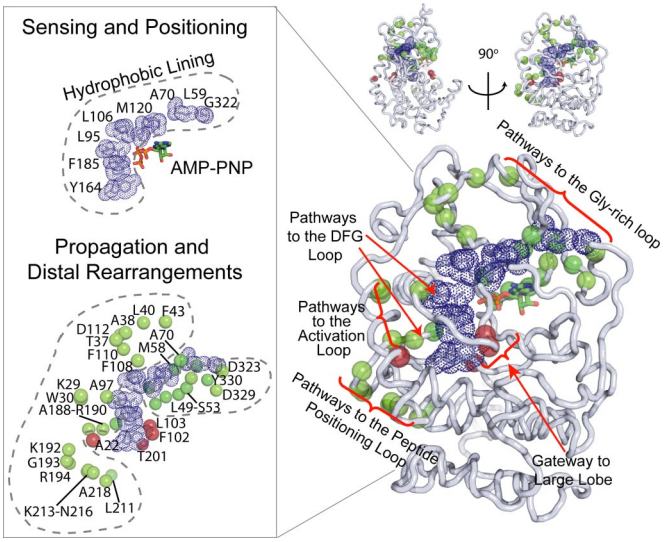

Fig. 4. Proposed model for the allosteric network of interactions in wild-type PKA-C. Blue, residues of the hydrophobic lining; green, residues showing the contiguous network of interactions located within van der Waals radii from the hydrophobic lining; red, residues showing noncontiguous interactions located outside of the van der Waals contacts.

propagate signals to and from the glycine-rich, activation, Asp-Phe-Gly, and peptide-positioning loops at the entrance of the active site. We also detected noncontiguous propagation for a small subset of residues in distal sites, for which no clear pathway of interaction can be traced. In the wild-type enzyme, two regions display relatively large $\Delta\delta$ values. The first is located at the N terminus (≈24 Å from the nucleotide-binding pocket). The second region, located at ≈12 Å from the nucleotide-binding pocket, comprises F100 and F102, which bridge the small and large lobes (18), and demonstrates that the signal is transmitted across the two lobes of the enzyme. A possible explanation for noncontiguous signaling is that small local conformational changes add up and culminate in crucial regions of the enzyme, providing a long-range intramolecular signaling mechanism up to ≈24 Å from the nucleotide-binding site (see red residues in Fig. 4). In contrast, the Y204A mutation causes an overall rearrangement of the allosteric communication between the two lobes of the enzyme upon nucleotide binding and an interruption of this communication upon substrate binding.

To what extent do the chemical-shift changes reflect the conformational transitions to the states observed by x-ray crystallography? Chemical-shift changes encompass several different phenomena (conformational interconversion, different binding modes, binding kinetics, electrostatics, and hydrogen bonding) (43–46), and in the absence of spin-relaxation measurements to supplement these results, it is difficult to quantify the different contributions. However, we found a direct correlation between the measured $\Delta\delta$ values and the difference in the Cα atomic coordinates between the apo (1J3H) and intermediate (1BKX) structures and between the intermediate (1BKX) and closed (1ATP) structures (SI Fig. 8). The overall trend is remarkably similar, which supports the hypothesis that allostery is partially mediated by conformational changes throughout the entire enzyme. These observations are in agreement with other studies carried out by using fluorescence anisotropy (18). This does not exclude the role of protein dynamics for the positive allosteric cooperativity. In fact, the crystal structures for the closed forms of Y204A and wild-type PKA-C are identical (21), although solution data indicate Y204A is more dynamic (23). This increase in dynamics may contribute to the disruption of the allosteric network and decoupling of the binding cooperativity. Further analyses of NMR spin relaxation properties supplemented by solvent accessibility and thermostability are needed to determine the relative importance of dynamics and conformational changes in the positive allosteric cooperativity of the C-subunit.

The modern view of molecular allostery recognizes the existence of a dynamic structural ensemble of the protein native states (47–51). Our data suggest the reshaping of the allosteric energy landscape through ligand binding: the population of states, which are encoded in the apo enzyme shift in the presence of ligand to generate positive cooperativity. This work demonstrates that PKA-C is an exquisite example of allostery and communication networks between distal regions. These findings may serve as a paradigm for describing long-range coupling in other protein kinases.

Methods

Sample Preparation. PKA-C expression and activity assays were performed as previously described (52, 53) (details are provided in the *SI Text* and SI Fig. 9). NMR samples consisted of 0.44 and 0.63 mM of wild-type C subunit for the forward and reverse titrations, respectively. Samples for the mutant enzyme were ≈0.24 mM for the forward and reverse titrations. All samples were prepared in 20 mM KH_2PO_4, 10 mM DTT, 180 mM KCl, 10 mM $MgCl_2$, 1 mM NaN_3, and 5% ^2H_2O.

NMR Assignments and Ligand Titrations. NMR experiments were carried out by using Varian Inova spectrometers operating at 800.24 or 599.71 MHz and equipped with triple-resonance cryogenic probes. Backbone resonance assignments for the wild-type enzyme were carried out by using HNCA, HN(CO)CA, HNCACB, HNCO, and HN(CA)CO experiments on $^2H/^{15}N/^{13}C$-labeled PKA samples at 300 K. Assignments were also assisted by selective ^{15}N amino acid labeling. These samples were titrated with both ligands to determine assignments for the bound states. SI Tables 3 and 4 summarize all experiments and acquisition parameters. Our resonance assignments compare well with the previous partial (55%) assignment obtained by Langer *et al.* (54). Spectra for the Y204A samples were virtually superimposable with resonances of wild-type enzyme; thus, assignments in this case were based on comparison (overlay of spectra are provided in SI Fig. 10). NMR data were processed and visualized by using the software NMRPipe (55) and SPARKY (56). Chemical-shift perturbations from NMR titrations were quantified using Eq. **1**,

$$\Delta\delta = \sqrt{\Delta\delta_H^2 + (0.154\Delta\delta_N)^2}, \qquad [1]$$

where $\Delta\delta$ is the combined chemical shift, and $\Delta\delta_H$ and $\Delta\delta_N$ are the differences of ^1H and ^{15}N chemical shifts, respectively, between the first and last points of the titrations. The weighting factor for the ^{15}N chemical shift has been previously described (24).

Assuming a 1:1 enzyme:ligand ratio (3, 4), K_d values were determined by a nonlinear fit (Eq. **2**) of resonances in fast exchange between free and bound enzyme (57):

$$\Delta\Omega_i = \frac{K_d + [L_T] + [E_T] - \sqrt{(K_D + [L_T] + [E_T])^2 - 4[L_T][E_T]}}{2[E_T]}\,\Delta\Omega, \qquad [2]$$

where $[E]_T$ and $[L]_T$ are total concentrations of enzyme and ligand added, respectively, and $\Delta\Omega_i$ and $\Delta\Omega$ are the chemical-shift differences between the observed and initial and final and initial resonances, respectively. Nonlinear least-squares fitting of the quadratic equation to the data was performed by using Mathematica software (39). The calculation for the dissociation constants in the Michaelis complex, which accounts for the small amount of free enzyme, is described in the *SI Text*.

ACKNOWLEDGMENTS. We thank Prof. L. E. Kay, Dr. V. Tugarinov, and Dr. M. Tonelli for sharing pulse sequences. This work was supported by the National Institutes of Health (Grants GM64742 and HL080081 to G.V., GM19301 to S.S.T., and GM08700 to L.R.M) and the American Heart Association (Grants 0515491Z to N.J.T. and 0615546Z to L.R.M). National Science Foundation funding (Grant BIR-961477) was provided to the University of Minnesota NMR

Facility. The NMR Facility at Madison is supported by the National Institutes of Health (Grants P41RR02301, P41GM66326, RR02781, and RR08438), the National Science Foundation (Grants DMB-8415048, OIA-9977486, and BIR-9214394), and the U.S. Department of Agriculture.

1. Manning G, Whyte DB, Martinez R, Hunter T, Sudarsanam S (2002) *Science* 298:1912–1934.
2. Tchieu JH, Fana F, Fink JL, Harper J, Nair TM, Niedner RH, Smith DW, Steube K, Tam TM, Veretnik S, *et al.* (2003) *Nucleic Acids Res* 31:342–344.
3. Knighton DR, Zheng J, Eyck LFT, Xuong NH, Taylor SS, Sowadski JM (1991) *Science* 253:414–420.
4. Knighton DR, Zheng JH, Ten Eyck LF, Ashford VA, Xuong NH, Taylor SS, Sowadski JM (1991) *Science* 253:407–414.
5. Iyer GH, Garrod S, Woods VL, Jr, Taylor SS (2005) *J Mol Biol* 351:1110–1122.
6. Zhang J, Ma Y, Taylor SS, Tsien RY (2001) *Proc Natl Acad Sci USA* 98:14997–15002.
7. Burns-Hamuro LL, Ma Y, Kammerer S, Reineke U, Self C, Cook C, Olson GL, Cantor CR, Braun A, Taylor SS (2003) *Proc Natl Acad Sci USA* 100:4072–4077.
8. Vigil D, Blumenthal DK, Taylor SS, Trewhella J (2006) *J Mol Biol* 357:880–889.
9. Taylor SS, Kim C, Vigil D, Haste NM, Yang J, Wu J, Anand GS (2005) *Biochim Biophys Acta* 1754:25–37.
10. Pervushin K, Riek R, Wider G, Wuthrich K (1997) *Proc Natl Acad Sci USA* 94:12366–12371.
11. Boehr DD, McElheny D, Dyson HJ, Wright PE (2006) *Science* 313:1638–1642.
12. Boehr DD, Dyson HJ, Wright PE (2006) *Chem Rev* 106:3055–3079.
13. Taylor SS, Radzio-Andzelm E, Madhusudan, Cheng X, Eyck LFT, Narayana N (1999) *Pharmacol Ther* 82:133–141.
14. Iyer GH, Moore MJ, Taylor SS (2005) *J Biol Chem* 280:8800–8807.
15. Aimes RT, Hemmer W, Taylor SS (2000) *Biochemistry* 39:8325–8332.
16. Taylor SS, Haste NM, Ghosh G (2005) *Cell* 122:823–825.
17. Burns-Hamuro LL, Barraclough DM, Taylor SS (2004) *Methods Enzymol* 390:354–374.
18. Johnson DA, Akamine P, Radzio-Andzelm E, Madhusudan M, Taylor SS (2001) *Chem Rev* 101:2243–2270.
19. Narayana N, Cox S, Shaltiel S, Taylor SS, Xuong N (1997) *Biochemistry* 36:4438–4448.
20. Lew J, Taylor SS, Adams JA (1997) *Biochemistry* 36:6717–6724.
21. Yang J, Ten Eyck LF, Xuong NH, Taylor SS (2004) *J Mol Biol* 336:473–487.
22. Moore MJ, Adams JA, Taylor SS (2003) *J Biol Chem* 278:10613–10618.
23. Yang J, Garrod SM, Deal MS, Anand GS, Woods J, Virgil L, Taylor S (2005) *J Mol Biol* 346:191–201.
24. Tugarinov V, Kay LE (2003) *J Mol Biol* 327:1121–1133.
25. Fersht A (1999) *Structure and Mechanism in Protein Science* (Freeman, New York).
26. Gerstein M, Lesk AM, Chothia C (1994) *Biochemistry* 33:6739–6749.
27. Linse S, Chazin WJ (1995) *Protein Sci* 4:1038–1044.
28. Maler L, Blankenship J, Rance M, Chazin WJ (2000) *Nat Struct Biol* 7:245–250.
29. Volkman BF, Lipson D, Wemmer DE, Kern D (2001) *Science* 291:2429–2433.
30. Kern D, Zuiderweg ER (2003) *Curr Opin Struct Biol* 13:748–757.
31. Eisenmesser EZ, Millet O, Labeikovsky W, Korzhnev DM, Wolf-Watz M, Bosco DA, Skalicky JJ, Kay LE, Kern D (2005) *Nature* 438:117–121.
32. Leung DW, Rosen MK (2005) *Proc Natl Acad Sci USA* 102:5685–5690.
33. Popovych N, Sun S, Ebright RH, Kalodimos CG (2006) *Nat Struct Mol Biol* 13:831–838.
34. Ferguson AD, Amezcua CA, Halabi NM, Chelliah Y, Rosen MK, Ranganathan R, Deisenhofer J (2007) *Proc Natl Acad Sci USA* 104:513–518.
35. Das R, Esposito V, Abu-Abed M, Anand GS, Taylor SS, Melacini G (2007) *Proc Natl Acad Sci USA* 104:93–98.
36. Stevens SY, Sanker S, Kent C, Zuiderweg ER (2001) *Nat Struct Biol* 8:947–952.
37. Das R, Abu-Abed M, Melacini G (2006) *J Am Chem Soc* 128:8406–8407.
38. Velyvis A, Yang YR, Schachman HK, Kay LE (2007) *Proc Natl Acad Sci USA* 104:8815–8820.
39. Wolfram Research (2005) *Mathematica* (Wolfram Research, Champaign, IL).
40. Sprangers R, Gribun A, Hwang PM, Houry WA, Kay LE (2005) *Proc Natl Acad Sci USA* 102:16678–16683.
41. Clarkson MW, Gilmore SA, Edgell MH, Lee AL (2006) *Biochemistry* 45:7693–7699.
42. Kornev AP, Haste NM, Taylor SS, Ten Eyck LF (2006) *Proc Natl Acad Sci USA* 103:17783–17788.
43. Sitkoff D, Case DA (1997) *J Am Chem Soc* 119:12262–12273.
44. Revington M, Holder TM, Zuiderweg ER (2004) *J Biol Chem* 279:33958–33967.
45. Matsuo H, Walters KJ, Teruya K, Tanaka T, Gassner GT, Lippard SJ, Kyogoku Y, Wagner G (1999) *J Am Chem Soc* 121:9903–9904.
46. Hellstern S, Pegoraro S, Karim CB, Lustig A, Thomas DD, Moroder L, Engel J (2001) *J Biol Chem* 276:30845–30852.
47. Freire E (1999) *Proc Natl Acad Sci USA* 96:10118–10122.
48. Kumar S, Ma B, Tsai CJ, Sinha N, Nussinov R (2000) *Protein Sci* 9:10–19.
49. Hammes GG (2002) *Biochemistry* 41:8221–8228.
50. Hammes-Schiffer S, Benkovic SJ (2006) *Annu Rev Biochem* 75:519–541.
51. Swain JF, Gierasch LM (2006) *Curr Opin Struct Biol* 16:102–108.
52. Yonemoto WM, McGlone ML, Slice LW, Taylor SS (1991) *Methods Enzymol* 200:581–596.
53. Cook PF, Neville ME, Vrana KE, Hartl FT, Roskoshi R (1982) *Biochemistry* 21:5794–5799.
54. Langer T, Vogtherr M, Elshorst B, Betz M, Schieborr U, Saxena K, Schwalbe H (2004) *ChemBioChem* 5:1508–1516.
55. Delaglio F, Grzesiek S, Vuister GW, Zhu G, Pfeifer J, Bax A (1995) *J Biomol NMR* 6:277–293.
56. Goddard TD, Kneller DG (2006) *SPARKY* 3.113 (University of California, San Francisco).
57. Johnson PE, Tomme P, Joshi MD, McIntosh LP (1996) *Biochemistry* 35:13895–13906.